Published paper

M. Kovačić, S. Stipetić, Z. Hanić and D. Žarko, "Small-Signal Calculation of Common-Mode Choke Characteristics Using Finite-Element Method," in *IEEE Transactions on Electromagnetic Compatibility*, vol. 57, no. 1, pp. 93-101, Feb. 2015.

http://dx.doi.org/10.1109/TEMC.2014.2362998

Small Signal Calculation of Common Mode Choke Characteristics Using Finite Element Method

Marinko Kovacic, *Student Member,* Stjepan Stipetic, *Student Member,* Zlatko Hanic, *Student Member,* Damir Zarko, *Member*

***Abstract*—This paper presents a finite element method approach to calculation of the common mode choke impedance over a wide frequency range. The proposed method involves a 3D electrostatic finite element calculation of each turn-to-turn and turn-to-core capacitance, and their usage as electric circuit lumped parameters in the 3D time-harmonic magnetic finite element calculation of the common mode choke impedance. It also takes into account the variation of the nanocrystalline core permeability and losses with frequency up to 100 MHz. The proposed methodology is used for calculation of the common mode, open mode and differential mode impedance characteristic for single-phase and three-phase common mode choke. Results are compared with measurements.**

***Index Terms*—Circuit analysis, Electromagnetic analysis, Electromagnetic compatibility, Finite element method, Inductors, Magnetic cores, Magnetic materials, Permeability, Power filters**

I. INTRODUCTION

DUE to the switching of power semiconductor devices at high frequency and the presence of stray capacitances, common mode and differential mode noise occurs in power electronic circuits. Common mode noise generates current flow in the same direction through supply wires which is called common mode current (Fig. 1). On the other hand, differential noise generates current in the opposite direction through supply wires which is called differential mode current. Both common mode and differential mode current cause electromagnetic interference (EMI) in the radio frequency part of the electromagnetic spectrum. Today's regulations concerning electromagnetic compatibility (EMC) require restriction of EMI. This is achieved by using EMI filters. The part of the EMI filter that suppresses common mode current is the common mode choke (CMC). In the simplest case, single-phase CMC consists of two coils wound in the opposite direction on a permeable core. Differential current flowing through each coil will generate magnetic flux components in the core in the opposite directions thus cancelling each other (Fig. 2) and resulting in low inductance of the coil, while common mode current will generate flux components in the same direction resulting in high inductance of the coil. Therefore, CMC will attenuate common mode currents and at the same time will practically not affect differential mode current.

Marinko Kovacic, Stjepan Stipetic, Zlatko Hanic and Damir Zarko are with the University of Zagreb, Faculty of Electrical Engineering and Computing, Department of Electric Machines, Drives and Automation, Zagreb, Croatia (e-mail: marinko.kovacic@fer.hr, stjepan.stipetic@fer.hr, zlatko.hanic@fer.hr, damir.zarko@fer.hr).

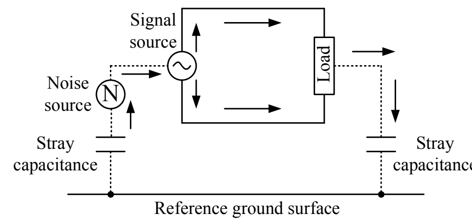

Fig. 1. Common mode noise and direction of common mode current in power electronic devices

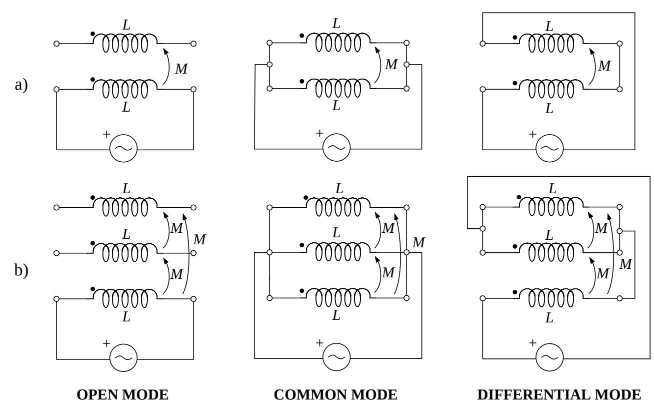

Fig. 2. Connection of the choke's windings for measurement of open mode, common mode and differential mode impedance for (a) single-phase CMC (b) three-phase CMC. Voltage source is impedance analyzer.

In order to properly design a CMC it is crucial to obtain its impedance characteristic. Our previous paper [1] deals with the development of the analytical model for calculation of the CMC impedance. The analytical calculation is very fast and can be used in the optimization, but the final result has to be checked using a more accurate method. This paper presents a 3D finite element calculation of the CMC impedance as a means of verification of the analytically calculated results.

There are many papers dealing with FE modeling of the magnetic components. Pleite *et. al* [2] give an overview of FE techniques for magnetic components at high frequencies, which include the effects of parasitic capacitance and frequency dependent complex mutual inductance on calculation of impedance. Chen *et. al* [3] use the FE method to investigate the influence of the magnetic flux generated by differential current on the CMC impedance. Authors in [4]–[11] analyze the calculation of the AC winding resistance which takes into account proximity and skin effects.

Prieto *et. al* [12] propose a new method for the simulation of the magnetic field distribution. Instead of solving a 3D FE problem, they solve two 2D FE problems to obtain the magnetic field distribution. Their methodology is compared with experimental results. Poulichet *et. al* [13] develop a high frequency model of the current transformer (100 kHz to 55 MHz). They have subdivided the current transformer into sections. Each section contains a core, and a few secondary turns. The inductances and capacitances of every section were calculated using FEM. After parameter calculation, an electrical model is formed which unifies the subdivided sections. However, the complex permeability was not been used and core losses were not been modeled. The model and the experimental results are showing poor matching. Bouissou et al. [14] use 3D FE analysis with circuit equations to simulate the power transformer transient condition such as sudden three-phase short-circuit on the secondary winding. The use of passive electric components such as resistors, capacitors and inductors in the FE analysis is described in [15], [16].

In order to reduce the complexity of the FE mesh Tran *et. al* [17] use the FE method coupled with the partial element equivalent circuit method (PEEC) to solve the time-harmonic problems involving multiple thin conductors and ferromagnetic core. The PEEC has been used to model the conductors while FE has been used to model the ferromagnetic core. The new formulation is particularly well suited for modeling complex electromagnetic devices including a large number of conductors. Kovacevic *et. al* [18] used the PEEC model of a toroidal magnetic inductor to calculate it's impedance over frequency range from 40 Hz to 110 MHz. The result showed good agreement with measurement up to the first resonant frequency.

Basic design equations for determination of main core dimensions and the number of turns of a CMC are described in [19]. More accurate modeling of the CMC requires the inclusion of parasitic effects such as parasitic capacitance, leakage inductance and core losses [20]–[22]. Massarini and Kazimierczuk in [23] present an analytical method for calculation of parasitic capacitances of inductors which could also be applied on multilayer inductors. Yu and Holmes [24] calculate partial capacitances between each turn on the ferrite rod using 2D and 3D FE analysis. Shishan *et. al* [25] also use the similar approach in order to calculate the partial turn-to-turn capacitance on a toroidal type core. They have concluded that 2D FE problem is not applicable for modeling of turn-to-turn capacitance due to large influence of fringing effects and therefore it is advisable to use the 3D model. Behavioral model that describes input-output relations of a CMC has been developed in [26] by fitting measurement data to the proposed model. Similar approach has been used in [27] to extract parameters of equivalent circuit for high frequency from measurement data.

The FE method proposed in this paper relies on calculation of parasitic partial capacitances (turn-to-turn and turn-to-core) using 3D electrostatic FE solver and the utilization of those capacitances as lumped parameters in a 3D time-harmonic model. Thus the user can conduct a series of calculations by varying the source frequency.

The method presented in this paper uses the subdivision of choke windings into single turns. The parasitic capacitances have been connected between each turn-to-turn and turn-to core node as it has been done in the analytical model in [1]. The parameters such as turn self inductance, mutual inductance to other turns and core losses are calculated by FE analysis in the same manner as it has been done analytically.

The FE approach is not as fast as the analytical method or the PEEC method, but it is very useful for observing the electromagnetic state of the CMC more accurately even when the geometry is complicated. It can also be used as a referent method in the CMC analytical model development process.

II. Material Properties

Nanocrystalline tape-wound cores are widely used in common mode choke applications due to their unique combination of properties. Usage of nanocrystalline cores instead of ferrite cores can significantly reduce the volume of EMI filters [28]. The properties of nanocrystalline soft magnetic alloys (e.g. VITROPERM, FINEMET) are very well described in literature [29], [30].

The properties of the core material are essential for correct modeling of the choke inductance since core permeability can be modeled to take into account the magnetization of the core and the power dissipation due to losses, which are both reflected on the real and imaginary part of the choke impedance. The electrical properties (permittivity) and accurate dimensions of foil and core plastic encapsulation box or epoxy coating must also be known for correct calculation of the winding capacitance.

For high frequency applications it is very important to use complex permeability $\mu^* = \mu' - j\mu''$ for correct modeling of materials. Even if the wire resistance is neglected, coil still has the real part of the impedance due to core losses. The complex self-impedance of a single turn wound around the toroidal core can be represented as a serial combination of inductance and resistance

$$j\omega L = j\omega(\mu' - j\mu'')\frac{h}{2\pi}\ln\left(\frac{D}{d}\right) = j\omega L_s + R_s \tag{1}$$

where h is the axial height, D is the outer diameter and d is the inner diameter of the core.

In this paper, the core material is modeled as solid with no lamination and conductance included since eddy current losses are modeled by complex permeability. The laminations are modeled by introducing the core fill factor k_{Fe} which is the ratio of the effective core area and the real (geometric) area. It is required to scale the complex permeability (real and imaginary part) with k_{Fe} factor using the expression $\mu_{equ}(\omega) = k_{Fe}\mu(\omega)$, where $\mu(\omega)$ is the actual permeability of the material and $\mu_{equ}(\omega)$ is the equivalent permeability used in both analytical and FE calculation to model the lamination [31]. The core fill factor for VAC VITROPERM is assumed to be $k_{Fe} = 0.8$ according to datasheets and literature [32].

For modeling purposes it is best to use the manufacturer's measured data for the complex permeability, but that information over broadband frequency range (e.g. 100 kHz - 100 MHz) is rarely available.The core manufacturers usually provide figures with frequency vs. permeability data which are almost unusable for serious modeling of the material. The table data is very rare and often given for frequencies up to maximum 1 MHz. The field of interest for design or application of CMC's can extend up to 50 MHz or 100 MHz to catch higher resonances or even to reach the first resonance. One can extract several points from such figure and try to fit the data for frequencies higher than available, but extrapolation could be very questionable. Dossoudil and Olah [33] have measured the complex permeability of ferrite over the frequency range 1 MHz to 1 GHz using the high frequency coaxial line sample holder of their own design. Some papers deal with the concept of analytical wide frequency complex permeability function. The frequency dependent absolute complex permeability $\mu(s)$ is somewhere given as a complex $\tanh$ function [34]–[36]. This equation fits the table data of most manufacturers very well up to approximately 1 MHz, but some corrections are needed for higher frequencies. Lebourgeois *et. al.* [37] have measured the complex permeability vs. frequency between 10 kHz and 1 GHz of a soft nanocrystalline magnetic material (FINEMET composition) and showed that eddy current model is not sufficient to explain the decrease of permeability at high frequencies. Weber *et. al.* [38] have modeled the complex permeability with analytical functions. Van den Bossche, Valchev *et. al.* [32], [39], [40] proposed a wide complex permeability function for linear magnetic materials in which both the power loss, the reactive power and the complex permeability of soft magnetic material cores are described.

The nanocrystalline material has a complex permeability angle $\arctan(\mu''/\mu')$ larger than 45° at very high frequencies, which means that the material is more resistive than inductive. Vacuumschmelze figures and table data [41] show that the final complex permeability angle approaches 90° (the same is also found in most of the above mentioned models and measurements). The analytical determination of the final angle is a very complex problem and it has not been considered in this paper. Nevertheless, the FE model presented in this paper is not sensitive to this parameter due to the fact that impedance behavior at high frequencies is mainly determined by winding capacitance and leakage reactance rather than by coil self inductance and equivalent loss resistance. This paper does not deal with the frequency behavior of the complex permeability, but it is needed along with the correct geometry for successful modeling and impedance calculation. The frequency behavior of complex permeability used in the FE model has been described by the modified classical eddy current formula. The optional final angle can be obtained by multiplying complex $\tanh$ function with the terms of the known phase shift. The hyperbolic tangent function results in the phase shift of 45° and from the Bode plot theory it is known that every term of the type $(1+\frac{j\omega}{\omega_{pi}})^{-\frac{1}{n}}$ shifts the phase for additional $45°/(n/2)$. The final angle of 90° can therefore be obtained by using three sixth root terms

$$\mu(s) = \mu_i \left[\frac{\tanh\left(\sqrt{s\sigma\mu_i}\frac{d}{2}\right)}{\sqrt{s\sigma\mu_i}\frac{d}{2}}\right] \cdot \frac{1}{\sqrt[6]{1+\frac{j\omega}{\omega_{p1}}}} \cdot \frac{1}{\sqrt[6]{1+\frac{j\omega}{\omega_{p2}}}} \cdot \frac{1}{\sqrt[6]{1+\frac{j\omega}{\omega_{p3}}}} \tag{2}$$

For the purpose of obtaining the frequency dependence of complex permeability used in the FE model, the table data of absolute values of relative complex permeability for Vacuumschmelze nanocrystalline cores has been used [42]. A surface fit has been used to obtain the absolute value of relative complex permeability at any frequency for a given initial relative permeability. Next, the optimization algorithm has been used to find parameters (σ, d, ω_{p1}, ω_{p2}, ω_{p13}) that satisfy (2) in the best possible way. It is possible to extrapolate the frequency dependence of complex permeability up to 100 MHz. Fig. 3 shows an example of the extrapolated complex permeability for the VACx425 nanocrystalline core obtained using the described method.

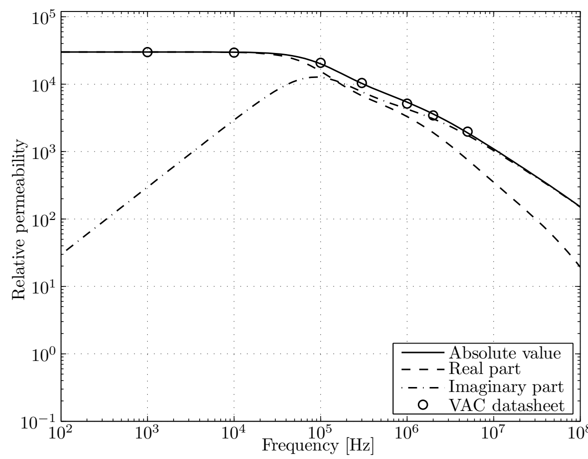

Fig. 3. Extrapolated complex permeability of the VACx425 nanocrystalline core in the frequency range 100 Hz to 100 MHz for initial relative permeability $\mu_{init} = 27000$

Due to lack of information regarding the exact value of the final angle of the complex permeability at very high frequencies, which has been assumed to be 90°, for accurate modeling (analytical or FEM) the data of the complex permeability should be known from either the measurement or directly from the manufacturer for the entire frequency range of interest (without extrapolation).

It should be noted that the calculation of the permeability described in this section does not take into account magnetic saturation. Therefore, the calculation of permeability is independent on current amplitude.

III. Finite Element Model of the CMC

The CMC has to be analyzed as both electrostatic and electromagnetic problem to accurately model the behavior at high frequencies. A straightforward approach would require simultaneous solving of Maxwell's equations for **B** and **E** fields, which would be complex to define and solve. The approach that has been used is to calculate parasitic capacitances using electrostatic FE model and afterwards insert them as lumped parameters into electromagnetic time-harmonic FE model coupled with an electric circuit.

It is useful to simplify the geometry using symmetries in the FE model. The symmetries also have to be satisfied from an electromagnetic point of view. The CMC can be simplified to one half of the original geometry, but cannot be simplified down to one quarter size due to interaction of the second winding and its parasitic capacitance in the high frequency range. Therefore, one half of the model is the most appropriate to use. The behavior of the choke can be modeled using only one half of the geometry for both capacitance and inductance calculations.

A. Finite Element Calculation of Capacitance

The electrostatic FE solver has been used to calculate the parasitic capacitances. The capacitance is assumed to remain constant over the entire frequency range so only static FE calculation is required. Electrostatic problem is defined by Laplace equation with corresponding boundary conditions.

$$\Delta\varphi = 0 \tag{3}$$

Every elementary turn has to be defined as an electrode. The electrode is modeled as the boundary condition with the constant value of electric potential. Since the core is conductive, it also has to be declared as an electrode to calculate the coil-to-core capacitance. It is of great importance to define the permittivity of the core's plastic coating or encapsulating material to calculate the coil-to-core capacitances correctly.

It is possible to calculate the capacitance between any of the two electrodes using FEM by applying a voltage to the observed electrode while all other electrodes are grounded. Upon solving the electrostatic FE problem one can notice that positive electric charge is distributed over the surface of the observed electrode. On all other electrodes, which are grounded, negative electric charge will be induced. The sum of charges on all electrodes in the model, including ground boundary, has to be zero. The partial capacitance between any of the two electrodes, where one is energized and one grounded, is given by

$$C_{ij} = \left|\frac{Q_j}{U_i}\right|, \qquad i \neq j \tag{4}$$

$$C_{ii} = \frac{2 \cdot |Q_i| - \sum\limits_{k=1}^{n} |Q_k|}{|U_i|}, \qquad i = j \tag{5}$$

where C_{ij} is the partial capacitance between i^{th} and j^{th} electrodes (non diagonal elements of the capacitance matrix), C_{ii} is the partial capacitance between i^{th} electrode and ground, Q_j is the induced charge on the j^{th} electrode, U_i is the voltage applied to the i^{th} electrode, and n is the number of electrodes in the model. It is necessary to carry out a series of n instances of FE calculations to calculate the entire partial capacitance matrix. In every instance only one electrode is energized while all other are set to ground potential.

B. Finite Element Calculation of Impedance

After a successful FE calculation of the partial capacitance matrix from the electrostatic FE model, it is possible to insert those capacitances as lumped parameters into magnetic time-harmonic FE model. The formulation of the magnetic time-harmonic FE problem is given by

$$\nabla \times \left[(\sigma + j\omega\varepsilon)^{-1} \nabla \times \mathbf{H}\right] + j\omega\mu\mathbf{H} = \mathbf{0} \tag{6}$$

which has to be solved for the magnetic field $\mathbf{H}$.

It is recommended to use one half of the model for electromagnetic field calculation due to the model symmetry. The core's protective plastic/epoxy casing is not used in magnetic calculation and it can be removed from the model since it is not conductive and has relative permeability equal to one.

The capacitances are inserted into a lumped equivalent circuit of the FE application. The lumped capacitances are connected to the coil terminals of the FE model. Only capacitances between two adjacent turns and the capacitances between core and turn are taken into account. All other capacitances in the model can be neglected since they are at least one order of magnitude smaller. For a three-phase CMC and for different operation modes, coils are connected in an analogue manner as shown in Fig. 2 b).

Fig. 4 shows an example of an equivalent circuit used for FE calculation of open mode impedance for single-phase CMC. Every coil modeled with FEM has ohmic resistance, and resistance due to core losses which is modeled with complex permeability and inductance. All the coils have complex mutual inductance due to complex permeability of the core.

The FE calculation is carried out using Infolytica MagNet 3D time-harmonic solver. The time-harmonic solver finds the time-harmonic magnetic field in and around current-carrying conductors in the presence of materials which can be conducting, magnetic, or both. The FE software does the time-harmonic analysis at one specified frequency. The sources and fields are represented by complex phasors. Theoretically, the time-harmonic analysis is only possible when all the materials in the problem are linear.

If a current source of 1 A RMS is used in the equivalent circuit and the model is solved using time-harmonic analysis, the voltage on the current source will numerically represent the value of the complex impedance which contains magnitude and phase. In order to obtain the impedance characteristic it is required to conduct a series of FE calculations by varying the current source frequency. In the vicinity of resonant frequencies it is required to refine the frequency step so that impedance characteristic can be calculated correctly.

This approach to the CMC impedance calculation reduces the need for simultaneous solving of both electric and magnetic field in one FE problem. The effects of the electric field are introduced by incorporating turn-to-turn and turn-to-core stray capacitances as lumped parameters into equivalent turn-wise circuit of the CMC winding which is later used for time-harmonic calculation of only magnetic field. This approach significantly reduces computational time.

C. The Use of the Half Symmetry Model in the Finite Element Analysis

Special precautions must be taken when calculating impedance characteristic using a half model of the common

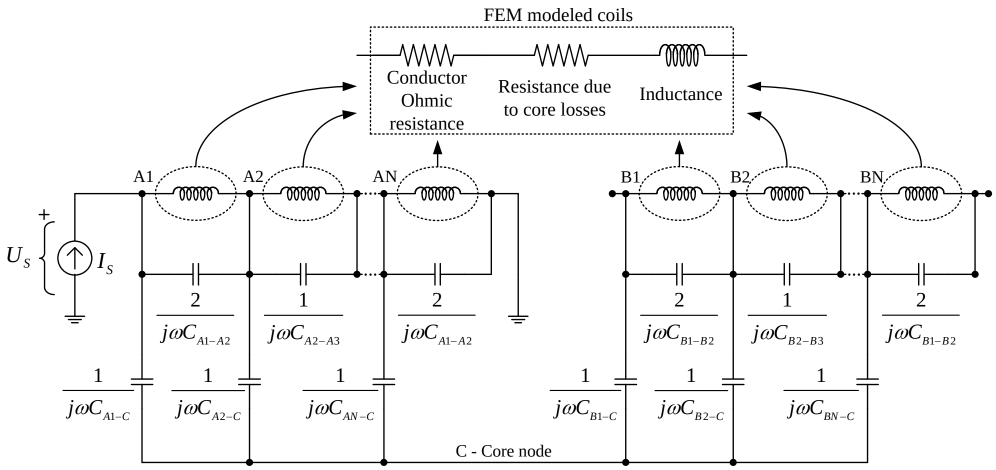

Fig. 4. Circuit diagram with turn-to-turn and turn-to-core capacitances inserted as lumped parameters

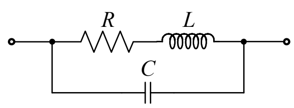

Fig. 5. Elementary RLC circuit

mode choke. The behavior of the half versus full model can be explained using a simple RLC circuit (Fig. 5). The resistance R represents the ohmic resistance of the coil wire and the equivalent resistance which takes into account the core losses by means of complex permeability.

The frequency dependence of the impedance of the RLC circuit shown in Fig. 5 in the case of full geometry model is given by

$$Z_{full} = \frac{R_{full} + j\omega L_{full}}{j\omega R_{full} C_{full} - \omega^2 L_{full} C_{full} + 1} \tag{7}$$

The values of partial capacitances in the capacitance matrix calculated from the half model and the value of the ohmic resistance are twice smaller than in the full model ($C_{half} = C_{full}/2$, $R_{half} = R_{full}/2$) due to the half length of the conductors. The inductance and the equivalent core loss resistance are also twice smaller ($L_{half} = L_{full}/2$) due to the twice smaller area of the iron core. Using these relations it is possible to write the relation for impedance of the half model

$$Z_{half} = \frac{\frac{R_{full}}{2} + j\omega \frac{L_{full}}{2}}{j\omega \frac{R_{full}}{2}\frac{C_{full}}{2} - \omega^2 \frac{L_{full}}{2}\frac{C_{full}}{2} + 1} \tag{8}$$

One can notice that impedance characteristic (8) of the half model is different from the impedance characteristic of the full model (7), not just in terms of magnitude, but also in terms of frequency response. In order to correctly obtain the behavior of the full model using half model, it is necessary to change the values of capacitances entered in the lumped network in Fig. 4. It is only possible to modify the lumped capacitances because inductances and resistances are inherent to the geometry of the model used in the electromagnetic FE calculation. The equivalent capacitance C_{equ} and the factor k_Z are introduced to equalize frequency characteristics of the half and the full model.

$$Z_{halfequ} = \frac{\frac{R_{full}}{2} + j\omega \frac{L_{full}}{2}}{j\omega \frac{R_{full}}{2} C_{equ} - \omega^2 \frac{L_{full}}{2} C_{equ} + 1} \tag{9}$$

It is possible to equalize relations (7) and (9) which yields

$$Z_{full} = k_Z \cdot Z_{halfequ} \tag{10}$$

for correcting the magnitude of the impedance and

$$\begin{aligned} \frac{R_{full} + j\omega L_{full}}{j\omega R_{full} C_{full} - \omega^2 L_{full} C_{full} + 1} &= \\ k_Z \cdot \frac{\frac{R_{full}}{2} + j\omega \frac{L_{full}}{2}}{j\omega \frac{R_{full}}{2} C_{equ} - \omega^2 \frac{L_{full}}{2} C_{equ} + 1} & \end{aligned} \tag{11}$$

for correcting the capacitance.

Therefore, to obtain the same frequency characteristic using half model it is necessary to use the following relations

$$\begin{aligned} k_z &= 2 \\ C_{equ} &= 2 \cdot C_{full} = 4 \cdot C_{half} \\ Z_{full} &= 2 \cdot Z_{halfequ} \end{aligned} \tag{12}$$

These relations indicate that in order to obtain the same frequency behavior of the half FE model as it would be with the full model, it is necessary to insert the partial capacitances from the half model electrostatic FE simulation multiplied by a factor of 4 ($C_{equ} = 4C_{half}$) into the equivalent circuit. The impedance of such equivalent half model has to be multiplied by the factor $k_Z = 2$ to emulate behavior of the full model. The use of the half model additionally shortens the calculation time.

IV. Final results

The finite element model has been tested using a VAC 6123x425 CMC by Vacuumschmelze (Fig. 6(a)) and custom wound single-layer three-phase CMC (Fig. 6(b)) and compared with measurements. The details for electrostatic and time-harmonic magnetic calculation are shown in tables I and

TABLE I
DETAILS FOR 3D ELECTROSTATIC FINITE ELEMENT MODELS

	Custom three-phase CMC	6123x425
No. of thetraedra	188343	172578
No. of edges	239120	217229
No. of field nodes	277373	251682
Polynomial order	2	2
Total memory allocated	444.9 MB	536.5 MB

TABLE II
DETAILS FOR 3D TIME-HARMONIC MAGNETIC FINITE ELEMENT MODELS

	Custom three-phase CMC	6123x425
No. of thetraedra	956984	575122
No. of edges	1129539	694303
No. of field nodes	4049908	1160630
Polynomial order	2	2
Total memory allocated	1.622 GB	1.363 GB

II. One electrostatic FE calculation typically takes about 5 seconds, and one time-harmonic magnetic FE calculation usually takes about 5 minutes on personal computer with Intel Core 2 Quad Q8200 (64-bit) 2.333 GHz processor and 6GB of random-access memory. However, calculation speed is dependent on computer performances.

VAC 6123x425 is a single layer CMC with rather low initial real permeability ($\mu_{init} = 27000$) and nine turns per coil. The initial real permeability has been determined using the value of the choke inductance L_s (marked as A_L in the VAC datasheet) at the frequency of 10 kHz obtained from the VAC datasheet. The complex permeability vs. frequency characteristic for this particular choke shown in Fig. 3 has been obtained as described in Section II. Double-layer VAC 6123x308 CMC by Vacuumschmelze has been rewound to a three-phase single layer CMC with six turns per phase. The complex permeability vs. frequency characteristic of the core has been measured with impedance analyzer with only one turn wound on the core. Initial permeability of the used core is $\mu_{init} = 96000$.

Tables III and IV show the capacitance calculation results obtained from electrostatic FE calculation. For VAC 6123x425 turns have been labeled from A1 to A9 for the first winding and B1 to B9 for the second winding. Similarly, turns for three-phase CMC have been labeled with A1 to A6, B1 to B6 and C1 to C6. Figure 7 shows the mesh and solution field for the case when core electrode is energized with 1 V and other electrodes were set to 0 V which was used for the calculation of turn-to-core capacitances.

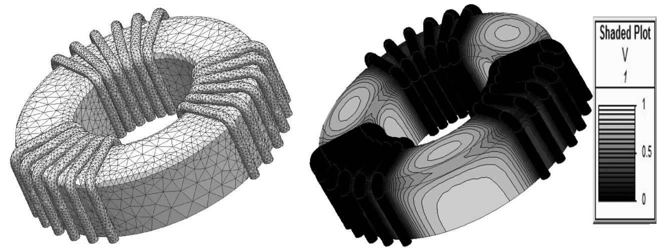

(a) (b)

Fig. 7. 3D FE model of three-phase CMC for electrostatic calculation of turn to core capacitances a) FE mesh b) distribution of electric potential

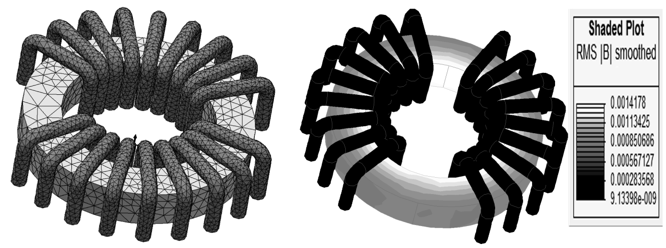

(a) (b)

Fig. 8. 3D FE model of the VAC 6123x425 CMC for time-harmonic magnetic calculation a) FE mesh b) distribution of magnetic flux density

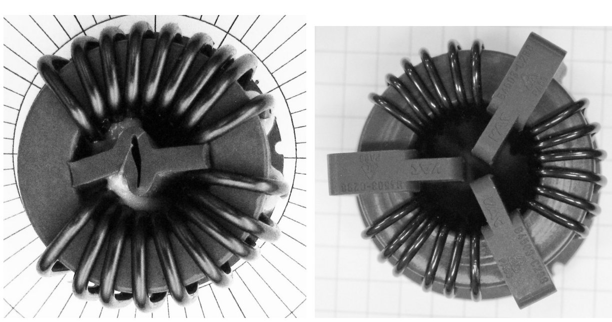

(a) (b)

Fig. 6. A photo of the common mode chokes used for calculation a) VAC 6123x425 CMC, b) custom three-phase single layer CMC

TABLE III
TURN-TO-TURN CAPACITANCES OBTAINED FROM 3D FE ELECTROSTATIC CALCULATION

Custom three-phase CMC			6123x425		
From	To	Capacitance, pF	From	To	Capacitance, pF
A1	A2	2.74	A1	A2	2.53
A2	A3	2.69	A2	A3	2.52
A3	A4	2.72	A3	A4	2.52
A4	A5	2.69	A4	A5	2.55
A5	A6	2.71	A5	A6	2.57
A6	B1	5.01	A6	A7	2.49
B1	B2	2.73	A7	A8	2.59
B2	B3	2.67	A8	A9	2.52
B3	B4	2.66	A9	B1	2.19
B3	B5	2.67	B1	B2	2.51
B5	B6	2.69	B2	B3	2.52
B6	C1	5.04	B3	B4	2.47
C1	C2	2.71	B4	B5	2.48
C2	C3	2.65	B5	B6	2.56
C3	C4	2.66	B6	B7	2.54
C4	C5	2.67	B7	B8	2.50
C5	C6	2.72	B8	B9	2.49

Impedance characteristic measurements have been conducted with Agilent 4395A impedance analyzer. The open mode impedance has been measured for VAC 6123x425 CMC and open, common and differential mode impedance has been measured for custom three-phase CMC for the frequency range between 10 kHz and 100 MHz. Although choke coils have not been wound perfectly, for simplicity the FE model assumes that every elementary turn is the same, the coils are fully symmetrical and all distances between turns and core are

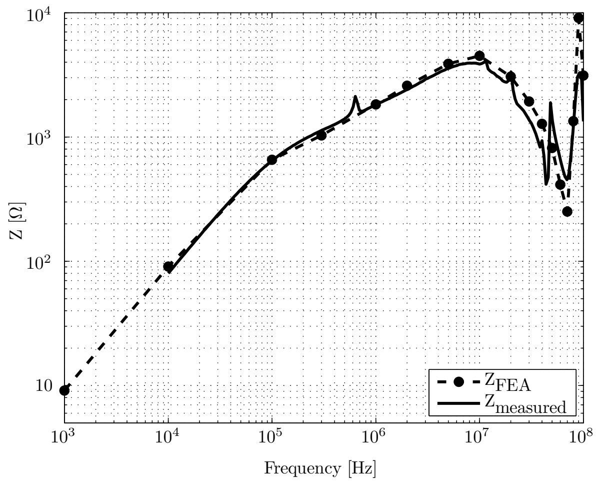

Fig. 9. Comparison of measured and calculated open mode impedance for VAC 6123x425 CMC

TABLE IV
TURN-TO-CORE CAPACITANCES OBTAINED FROM 3D FE ELECTROSTATIC CALCULATION

Custom three-phase CMC		6123x425	
Node	Capacitance, pF	Node	Capacitance, pF
A1	1.75	A1	3.46
A2	1.15	A2	2.77
A3	1.12	A3	2.75
A4	1.12	A4	2.74
A5	1.15	A5	2.72
A6	1.74	A6	2.72
B1	1.75	A7	2.75
B2	1.16	A8	2.75
B3	1.13	A9	3.33
B4	1.13	B1	3.43
B5	1.16	B2	2.79
B6	1.76	B3	2.75
C1	1.76	B4	2.79
C2	1.15	B5	2.69
C3	1.12	B6	2.72
C4	1.12	B7	2.75
C5	1.15	B8	2.73
C6	1.75	B9	3.37

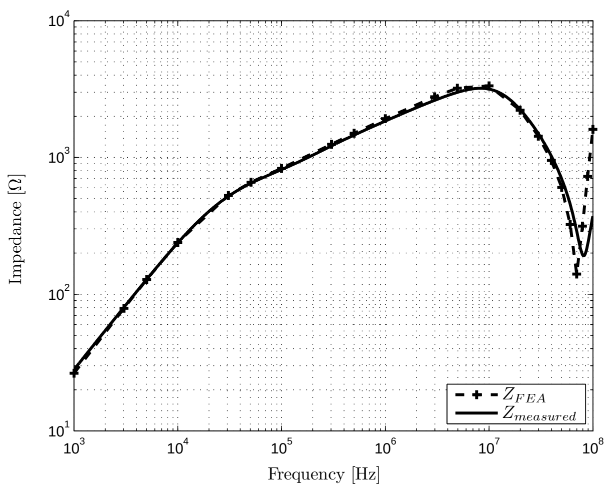

Fig. 10. Comparison of measured and calculated open mode impedance for three-phase CMC

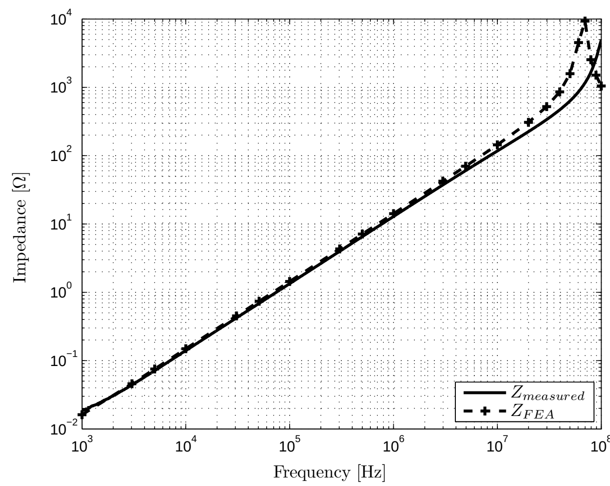

Fig. 12. Comparison of measured and calculated differential mode impedance for three-phase CMC

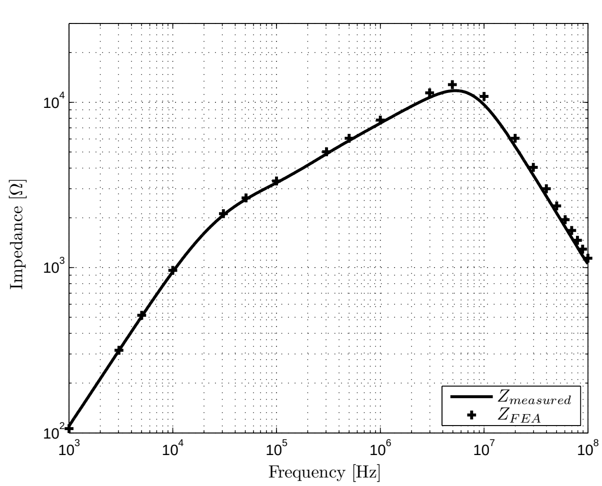

Fig. 11. Comparison of measured and calculated common mode impedance for three-phase CMC

constant for all turns (Fig. 7 and 8). The wire insulation is not taken into account due to limited computer memory available for generation of very detailed FE mesh.

Fig. 9 compares the impedance characteristics for the single phase VAC 6123x425 choke obtained in the following manners: calculated using FEA (Z_{FEA}) and measured using impedance analyzer ($Z_{measured}$). Figures 10, 11 and 12 show a comparison between FE calculated and measured open, common and differential mode impedance characteristics, respectively. It can be seen from Figs. 9 - 12 that resonance occurs. It occurs due interaction of leakage inductance and stray capacitances and it has been expected for both measurements and calculation.

V. CONCLUSION

A 3D finite element model for calculation of common mode choke impedance over a wide frequency range with lumped parameters related to individual turns of the coils wound on the toroidal core has been developed. This novel model combines the electrostatic simulation for calculation of parasitic capacitances and the time-harmonic magnetic simulation for calculation of the choke impedance. The time-harmonic simulation is combined with the equivalent electric circuit which contains parasitic capacitances as lumped parameters.

The other novelty of the model is the use of the simplified geometry with the choke cut in half which significantly reduces the calculation time. It has been shown in detail how to adjust the values of lumped parameters in the equivalent circuit in order to correctly calculate the CMC impedance for the full geometry.

The finite element calculation of the impedance characteristics has been done for a single layer single-phase and three-phase CMC for open, common and differential mode. The calculated and measured results show a good match. The key parameters for obtaining correct impedance calculation results at high frequencies are complex permeability frequency characteristics and parasitic capacitances. If nonlinear dielectric materials are used for the CMC design, a frequency variation of the capacitances should be considered. At high frequencies, the accuracy of the FE calculation also becomes sensitive to the exact geometry of the CMC.

Acknowledgment

Authors would like to thank Vacuumschmelze GmbH & Co. KG and Meglaj d.o.o. for providing CMC samples.

References

[1] M. Kovacic, Z. Hanic, S. Stipetic, S. Krishnamurthy, and D. Zarko, "Analytical wideband model of a common-mode choke," *Power Electronics, IEEE Transactions on*, vol. 27, no. 7, pp. 3173–3185, 2012.

[2] J. Pleite, R. Prieto, R. Asensi, J. Cobos, and E. Olías, "Modeling of magnetic components based on finite element techniques," in *Power Electronics Congress, 1996. Technical Proceedings. CIEP'96., V IEEE International*. IEEE, 1996, pp. 170–175.

[3] H. Chen, Z. Qian, S. Yang, and C. Wolf, "Finite-element modeling of saturation effect excited by differential-mode current in a common-mode choke," *Power Electronics, IEEE Transactions on*, vol. 24, no. 3, pp. 873–877, 2009.

[4] R. Wojda and M. Kazimierczuk, "Winding resistance of litz-wire and multi-strand inductors," *Power Electronics, IET*, vol. 5, no. 2, pp. 257–268, 2012.

[5] R. P. Wojda and M. K. Kazimierczuk, "Analytical optimization of solid round-wire windings," *Industrial Electronics, IEEE Transactions on*, vol. 60, no. 3, pp. 1033–1041, 2013.

[6] M. Kazimierczuk and R. Wojda, "Foil winding resistance and power loss in individual layers of inductors," *International Journal of Electronics and Telecommunications*, vol. 56, no. 3, pp. 237–246, 2010.

[7] R. P. Wojda and M. K. Kazimierczuk, "Proximity-effect winding loss in different conductors using magnetic field averaging," *COMPEL: The International Journal for Computation and Mathematics in Electrical and Electronic Engineering*, vol. 31, no. 6, pp. 1793–1814, 2012.

[8] R. Wojda and M. Kazimierczuk, "Optimum foil thickness of inductors conducting dc and non-sinusoidal periodic currents," *IET Power Electronics*, vol. 5, no. 6, pp. 801–812, 2012.

[9] R. P. Wojda and M. K. Kazimierczuk, "Magnetic field distribution and analytical optimization of foil windings conducting sinusoidal current," *Magnetics Letters, IEEE*, vol. 4, pp. 0 500 204–0 500 204, 2013.

[10] ——, "Analytical optimisation of solid-round-wire windings conducting dc and ac non-sinusoidal periodic currents," *IET Power Electronics*, vol. 6, no. 7, pp. 1462–1474, 2013.

[11] ——, "Analytical winding size optimisation for different conductor shapes using ampère's law," *IET Power Electronics*, vol. 6, no. 6, pp. 1058–1068, 2013.

[12] R. Prieto, J. Cobos, O. Garcia, P. Alou, and J. Uceda, "Model of integrated magnetics by means of double 2d finite element analysis techniques," in *Power Electronics Specialists Conference, 1999. PESC 99. 30th Annual IEEE*, vol. 1. IEEE, 1999, pp. 598–603.

[13] P. Poulichet, F. Costa, and É. Labouré, "High-frequency modeling of a current transformer by finite-element simulation," *Magnetics, IEEE Transactions on*, vol. 39, no. 2, pp. 998–1007, 2003.

[14] S. Bouissou, F. Piriou, C. Kieny, and G. Tanneau, "Numerical simulation of a power transformer using 3d finite element method coupled to circuit equation," *Magnetics, IEEE Transactions on*, vol. 30, no. 5, pp. 3224–3227, 1994.

[15] J. Vaananen, "Circuit theoretical approach to couple two-dimensional finite element models with external circuit equations," *Magnetics, IEEE Transactions on*, vol. 32, no. 2, pp. 400–410, 1996.

[16] N. Abe, J. Cardoso, and A. Foggia, "Coupling electric circuit and 2d-fem model with dommel's approach for transient analysis [of em devices]," *Magnetics, IEEE Transactions on*, vol. 34, no. 5, pp. 3487–3490, 1998.

[17] T. Tran, G. Meunier, P. Labie, Y. Le Floch, J. Roudet, J. Guichon, and Y. Maréchal, "Coupling peec-finite element method for solving electromagnetic problems," *Magnetics, IEEE Transactions on*, vol. 44, no. 6, pp. 1330–1333, 2008.

[18] I. Kovacevic, A. Musing, and J. Kolar, "PEEC modelling of toroidal magnetic inductor in frequency domain," in *Power Electronics Conference (IPEC), 2010 International*. IEEE, 2010, pp. 3158–3165.

[19] A. Muetze and C. Sullivan, "Simplified design of common-mode chokes for reduction of motor ground currents in inverter drives," *Industry Applications, IEEE Transactions on*, vol. 47, no. 6, pp. 2570–2577, 2011.

[20] L. Dalessandro, W. Odendaal, and J. Kolar, "Hf characterization and nonlinear modeling of a gapped toroidal magnetic structure," *Power Electronics, IEEE Transactions on*, vol. 21, no. 5, pp. 1167 –1175, 2006.

[21] M. Heldwein, L. Dalessandro, and J. Kolar, "The three-phase common-mode inductor: Modeling and design issues," *Industrial Electronics, IEEE Transactions on*, vol. 58, no. 8, pp. 3264–3274, 2011.

[22] M. Nave, "On modeling the common mode inductor," in *Electromagnetic Compatibility, 1991. Symposium Record., IEEE 1991 International Symposium on*. IEEE, 1991, pp. 452–457.

[23] A. Massarini and M. K. Kazimierczuk, "Self-capacitance of inductors," *Power Electronics, IEEE Transactions on*, vol. 12, no. 4, pp. 671–676, 1997.

[24] Q. Yu and T. Holmes, "A study on stray capacitance modeling of inductors by using the finite element method," *Electromagnetic Compatibility, IEEE Transactions on*, vol. 43, no. 1, pp. 88–93, 2001.

[25] W. Shishan, L. Zeyuan, and X. Yan, "Extraction of parasitic capacitance for toroidal ferrite core inductor," in *Industrial Electronics and Applications (ICIEA), 2010 the 5th IEEE Conference on*. IEEE, pp. 451–456.

[26] I. Stevanovic, S. Skibin, M. Masti, and M. Laitinen, "Behavioral modeling of chokes for emi simulations in power electronics," *Power Electronics, IEEE Transactions on*, vol. 28, no. 2, pp. 695–705, 2013.

[27] W. Tan, C. Cuellar, X. Margueron, and N. Idir, "A high frequency equivalent circuit and parameter extraction procedure for common mode choke in the emi filter," *Power Electronics, IEEE Transactions on*, vol. 28, no. 3, pp. 1157–1166, 2013.

[28] W. Thierry, S. Thierry, V. Benot, and G. Dominique, "Strong volume reduction of common mode choke for rfi filters with the help of nanocrystalline cores design and experiments," *Journal of Magnetism and Magnetic Materials*, vol. 304, no. 2, pp. e847 – e849, 2006.

[29] A. Roc'h and F. Leferink, "Nanocrystalline core material for high-performance common mode inductors," *Electromagnetic Compatibility, IEEE Transactions on*, vol. 54, no. 4, pp. 785–791, 2012.

[30] J. Petzold, "Advantages of softmagnetic nanocrystalline materials for modern electronic applications," *Journal of Magnetism and Magnetic Materials*, vol. 242, pp. 84–89, 2002.

[31] J. Sheppard, *Finite element analysis of electrical machines*. Kluwer Academic Publishers., 1995.

[32] A. V. d. Bossche and V. C. Valchev, *Inductors and Transformers for Power Electronics*, 1st ed. CRC Press, Mar. 2005.

[33] R. Dosoudil and V. Olah, "Measurement of complex permeability in the RF band," *Journal of Electrical Engineering*, vol. 45, no. 107s, pp. 97–100, 2004.

[34] J. Li, T. Abdallah, and C. Sullivan, "Improved calculation of core loss with nonsinusoidal waveforms," in *Industry Applications Conference, 2001. Thirty-Sixth IAS Annual Meeting. Conference Record of the 2001 IEEE*, vol. 4. IEEE, 2001, pp. 2203–2210.

[35] M. Antila, "Electromechanical properties of radial active magnetic bearings," Ph.D. dissertation, Helsinki University of Technology, Espoo, Finland, 1998.

[36] D. Meeker, E. Maslen, and M. Noh, “An augmented circuit model for magnetic bearings including eddy currents, fringing, and leakage,” *Magnetics, IEEE Transactions on*, vol. 32, no. 4, pp. 3219–3227, 2002.

[37] R. Lebourgeois, S. Bérenguer, C. Ramiarinjaona, and T. Waeckerlé, “Analysis of the initial complex permeability versus frequency of soft nanocrystalline ribbons and derived composites,” *Journal of Magnetism and Magnetic Materials*, vol. 254, pp. 191–194, 2003.

[38] S. Weber, M. Schinkel, E. Hoene, S. Guttowski, W. John, and H. Reichl, “Radio Frequency Characteristics of High Power Common-Mode Chokes,” in *IEEE Int. Zurich Symp. on Electromagnetic Compatibility*, 2005, pp. 1–4.

[39] A. Van den Bossche, V. Valchev, and M. De Wulf, “Wide frequency complex permeability function for linear magnetic materials,” *Journal of Magnetism and Magnetic Materials*, vol. 272, pp. 743–744, 2004.

[40] V. Valchev, A. Van den Bossche, and P. Sergeant, “Core losses in nanocrystalline soft magnetic materials under square voltage waveforms,” *Journal of Magnetism and Magnetic Materials*, vol. 320, no. 1-2, pp. 53–57, 2008.

[41] “Nanocrystalline VITROPERM EMC components,” *Vacuumschmelze GMBH und CO.KG*, 2010.

[42] W. R., “Nanocrystalline soft magnetic cores - an interesting alternative not only for high demanding applications,” *Sekels GmbH*, 2010.